PHYSICAL REVIEW B VOLUME 12, NUMBER 9 1 NOVEMBER 1975

Higher-order approximations for dynamical spin correlation functions in high-temperature paramagnets*

Peter A. Fedders
Arthur Holly Compton Laboratory of Physics, Washington University, St. Louis, Missouri 63130
(Received 5 May 1975)

A method of generating equations for dynamical two-point spin correlation functions for systems interacting via spin-spin interactions in the high-temperature limit is presented. The method is exact in the sense that all moments of the correlation functions are exact to order $1/Z$ where Z is the effective number of nearest spin neighbors. Thus the equations are formally exact in the limit of large dimensionality with nearest-neighbor interactions. As an example the method is applied to the isotropic Heisenberg paramagnet.

I. INTRODUCTION

In the past several years a number of papers containing first-principles calculations of dynamical spin correlation functions for paramagnetic systems interacting via spin-spin interactions have been published.[1-6] Most of these calculations are valid only in the high-temperature limit (where kT is much greater than any spin interaction energy), although some have been generalized to all temperatures at which the system is paramagnetic. Many of these calculations are based on a particular lowest-order decomposition that is usually called the Blume-Hubbard[1] approximation or the bubble[2] approximation. In an earlier paper[2] it was shown that this approximation is the first in a well-defined infinite sequence of self-consistent approximations. The resummation of the moment diagrams used to obtain these approximations is based on the ideas contained in the work of Wegner,[3] Resibois and De Leneer,[4] and especially Reiter[5] who first suggested this particular resummation.

However, even in the high-temperature limit, the bubble approximation is unsatisfactory in some respects. It produces spectral functions whose second moments are exact but whose higher moments are substantially incorrect. By using higher-order approximations,[2] one can generate spectral functions whose higher moments are exact to order $1/c$ where c is the effective number of spins in the range of interaction.[5] However, the complexity of the equations rapidly increases, and it does not appear to be feasible to go beyond the second-order approximation (which gives the fourth moment exact to order $1/c$). The defects of the bubble approximation are apparent for the Heisenberg paramagnet where the calculated line shape is quantitatively incorrect for some values of wave vectors, especially those near a zone edge. Recent calculations for the dipolar paramagnet are even more disappointing. The frequency-dependent spectral function for this system obtained from the bubble approximation is not a monotonic function of frequency and its peak is not at zero frequency.[7,8] This inconsistency with experimental fact is partially obscured by calculating the time-dependent free-induction-decay function because the zeroes of that calculated function are in reasonable good agreement with experiment. The next approximation above the bubble approximation in the sense of Ref. 2 has been tried and found not to remedy this nonmonotonic behavior.[9] From this we conclude that it may not be profitable to go to any further finite order in this scheme. In any case, it is not clear what effect approximations that reproduce a finite number of higher moments will have on the spectral function near zero frequency.

It is the purpose of this paper to exhibit a formalism which can be used to generate spectral functions which include parts of all of the "ladder" self-energy diagrams. The method is exact in the sense that *all* of the moments of the spectral function are exact to order $1/Z$ where Z is the effective number of *nearest* spin neighbors. More precisely, the method becomes exact for a spin system with only nearest-neighbor interactions as the dimensionality of the lattice becomes infinite. The quantity Z is not the same as the effective number of spins in the range of interaction, c, as defined by Reiter.[5] In fact there are many moment diagrams which contribute to lowest order in $1/c$ but not to lowest order in $1/Z$. On the other hand, for a system with only nearest-neighbor interactions, Z and c are equal. Although the method is valid only in the high-temperature limit, it may possibly be generalized to finite temperatures in a random-phase-approximation sense.

In the rest of this section we shall review certain aspects of the diagrammatic treatment of spin correlation functions and their moments needed for our present work. Section II contains the construction of the equations for the correlation functions. Although the method is applicable to all types of spin correlation functions with any spin-spin interactions, the details of the construction will refer to the dipole spin correlation function with isotropic

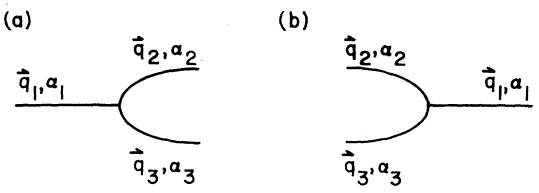

FIG. 1. Basic vertices for a general spin-spin interaction and the general form of their corresponding analytical expression. The quantities $\vec{q}_i$ are wave vectors and the quantities α_i are multipole indices.

Heisenberg exchange. In Sec. III we apply the formalism directly to the isotropic Heisenberg paramagnet and discuss applications to other systems.

In an earlier paper[2] we described a formalism for generating integral equations for spin correlation functions in the high-temperature limit based on Reiter's[5] diagrammatic analysis of the moments. A two-point time-dependent spin correlation function is defined as

$$G_{\alpha\beta}(\vec{l}-\vec{l}',\,t-t')=\langle A_\alpha(\vec{l},\,t)A^\dagger_\beta(\vec{l}',\,t')\rangle\,\Theta(t-t'), \tag{1}$$

where the angular brackets $\langle x\rangle$ denote the average value of x in the canonical ensemble, $\Theta(t)$ is the step function, and $A_\alpha(\vec{l},\,t)$ is the irreducible spin multipole operator[2,5] in the Heisenbergy representation at the lattice site $\vec{l}$. Since the system is translationally invariant in time and has the invariance of the crystal lattice under translations through a lattice vector, G can be transformed according to the usual prescription

$$G(\vec{l},\,t)=\frac{1}{N}\sum_{\vec{q}}\int_{-\infty}^{\infty}\frac{d\omega}{2\pi}\,G(\vec{q},\,\omega)\,e^{i\vec{q}\cdot\vec{l}-i\omega t}\,, \tag{2}$$

where N is the number of lattice sites and the summation is over all wave vectors $\vec{q}$ in the first Brillouin zone. It is further convenient to define a mass operator or self-energy $\Sigma_{\alpha\beta}(\vec{q},\,\omega)$ by the equation

$$\omega G_{\alpha\beta}(\vec{q},\,\omega)-\Sigma_{\alpha\gamma}(\vec{q},\,\omega)G_{\gamma\beta}(\vec{q},\,\omega)=i\delta_{\alpha\beta}, \tag{3}$$

where repeated Greek subscripts are summed over. In addition, one has real spectral functions $g(\vec{q},\,\omega)$ and $\Gamma(\vec{q},\,\omega)$ corresponding to $G(\vec{q},\,\omega)$ and $\Sigma(\vec{q},\,\omega)$,

$$G_{\alpha\beta}(\vec{q},\,\omega)=i\int_{-\infty}^{\infty}\frac{d\omega'}{\pi}\,\frac{g_{\alpha\beta}(\vec{q},\,\omega')}{\omega-\omega'+i\epsilon}\,, \tag{4a}$$

$$\Sigma_{\alpha\beta}(\vec{q},\,\omega)=\int_{-\infty}^{\infty}\frac{d\omega'}{\pi}\,\frac{\Gamma_{\alpha\beta}(\vec{q},\,\omega')}{\omega-\omega'+i\epsilon}$$

$$=\Pi_{\alpha\beta}(\vec{q},\,\omega)-i\Gamma_{\alpha\beta}(\vec{q},\,\omega)\,. \tag{4b}$$

It is easier to work with Σ than with G and our discussion will usually center around this function. The moments of Γ,

$$L_{\alpha\beta}(\vec{q},\,n)=\int_{-\infty}^{\infty}\frac{d\omega}{\pi}\,\omega^{n-2}\,\Gamma_{\alpha\beta}(\vec{q},\,\omega)\,, \tag{5a}$$

are easily related to the moments of g,

$$M_{\alpha\beta}(\vec{q},\,n)=\int_{-\infty}^{\infty}\frac{d\omega}{\pi}\,\omega^n\,g_{\alpha\beta}(\vec{q},\,\omega)\,. \tag{5b}$$

Reiter's[5] analysis for obtaining moments exact to order $1/c$ can be generalized in the following way. For any spin-spin interaction one forms matrix elements of the Liouville operator. This leads to basic vertices which can be represented diagrammatically as in Fig. 1 with a corresponding analytical expression. For example, for the dipole ($l=1$) multipole operators with isotropic exchange, the only possible vertices opening to the right are given in Fig. 2 along with their corresponding analytical expressions. The corresponding vertices opening to the left have the same analytical expression. In these equations,

$$V(\vec{q})=[\tfrac{1}{3}S(S+1)]^{1/2}\,J(\vec{q})/\hbar, \tag{6}$$

where J is the usual Heisenberg exchange energy.

The rules for $L_{\alpha\beta}(\vec{q},\,n)$ are (i) draw all distinct irreducible diagrams with n vertices which can be made from the basic vertices and which start with an α-type line and end with a β-type line. (ii) Label the initial line and final lines by $\vec{q}$. Label all internal lines by $\vec{q}_i$, α_i. (iii) Associate the appropriate expression from Fig. 1 with each vertex. (iv) Sum over all internal indices $\vec{q}_i$, α_i. The number of times a graph is counted is equal to the number of ways its internal vertices can be

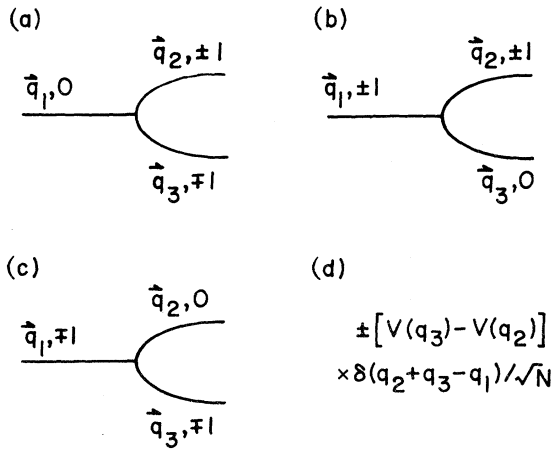

FIG. 1. Basic vertices opening to the right-hand side for the dipole ($l=1$) spin operators with isotropic Heisenberg exchange and the analytical expression associated with them in panel (d). The quantities $\vec{q}_i$, m_i refer to wave vector and azimuthal multipole index ($m=+1,\,0,\,-1$).

time ordered. This scheme yields $L_{\alpha\beta}(\vec{q}, n)$, which is exact to lowest order in $1/c$.

The rules for obtaining $\Sigma_{\alpha\beta}(\vec{q}, t)$ are quite similar.[2] In order to obtain the nth-order approximation for $\Sigma_{\alpha\beta}(\vec{q}, t)$, draw all skeleton diagrams having n vertices which can be made from the basic vertices and which start with an α-type line and end with a β-type line. In each skeleton diagram the internal lines are labeled in the same way as for the moment diagrams, but each vertex is also labeled by a time t_i, with t being the first vertex and zero being the last. In addition, in order to allow for nondiagonal correlation functions, each internal line can have different multipole indices α_i on its ends. Each line labeled $\vec{q}_i$ and going from vertex t_k to t_j starting with α_k and ending with α_j is replaced by $G_{\alpha_k\alpha_j}(\vec{q}_i, t_k - t_j)$. All internal $\vec{q}_i$ and α_i are summed over, all internal times t_i are integrated over, and a given diagram is multiplied by $(-i)^{n_v+1}$, when n_v is the number of internal vertices. The inclusion of static fields is trivial[2] and will not be included here.

II. CALCULATION

In this section we will first show how to extract those parts of each moment diagram which contributes to lowest order in $1/Z$. We will then show how to generate an integral equation for the spectral function which is consistent with these moments The Greek multipole indices α_i will be suppressed except where necessary for clarity.

First note that only the even moments of Γ are nonzero and that to lowest order $1/Z$, $L(\vec{q}, 2n)$ contains terms each with n factors consisting of $V^2(\vec{q})$ and/or $V^2(0)$, where

$$V^2(\vec{q}) = \frac{1}{N}\sum_{\vec{q}_1} V(\vec{q}_1)\, V(\vec{q} - \vec{q}_1) = \sum_{\vec{l}} [V(\vec{l})]^2 e^{i\vec{q}\cdot\vec{l}}, \quad (7)$$

and $V^2(0)$ is $V^2(\vec{q}=0)$. That is, each internal $\vec{q}_i$ must enter twice and only twice and must enter alone or with the external wave vector $\vec{q}$. It cannot enter in combination with another internal $\vec{q}_j$ with $j \neq i$. For example, with nearest-neighbor Heisenberg exchange,

$$V^2(\vec{q}) \propto Z\, V_0^2, \quad (8)$$

where V_0 is the nearest-neighbor interaction strength. Factors which have $V(\vec{q}_i)$ more than twice will contribute only to higher orders in $1/Z$. For example,

$$\frac{1}{N^2}\sum_{\vec{q}_1\vec{q}_2} [V(\vec{q}_1)]^2\, V(\vec{q}_2)\, V(\vec{q}_1 - \vec{q}_2)$$

$$= \sum_{\vec{l},\,\vec{l}'} [V(\vec{l})]^2\, V(\vec{l}')\, V(\vec{l} - \vec{l}') \quad (9)$$

is of order ZV_0^4 because the $\vec{l}'$ summation only includes sites which are nearest neighbors of both $\vec{l}$ and the origin. On the other hand, $[V^2(\vec{q})]^2$ or $V^2(0)\, V^2(\vec{q})$ is of order $Z^2 V_0^4$.

Using the fact that to lowest order in $1/Z$, $L(\vec{q}, 2n)$ can only include factors like those in Eq. (7), we shall first determine which skeleton diagrams contain all such terms. We shall then consider the nonskeleton irreducible diagrams and finally the integral equation for $g(\omega)$ which generates them. We start a general diagram with the vertex given in Fig. 3(a) which yields a factor $[V(\vec{q}_1) - V(\vec{q} - \vec{q}_1)]$. Notice that one leg of this vertex must end in a vertex opening to the right and the other must end in a vertex opening to the left, as in Fig. 3(c), except if we wish to close the diagram as in Fig. 3(b) which forms a complete skeleton diagram which cannot be added to. If both legs end in vertices opening to the right as in Fig. 3(d), a factor

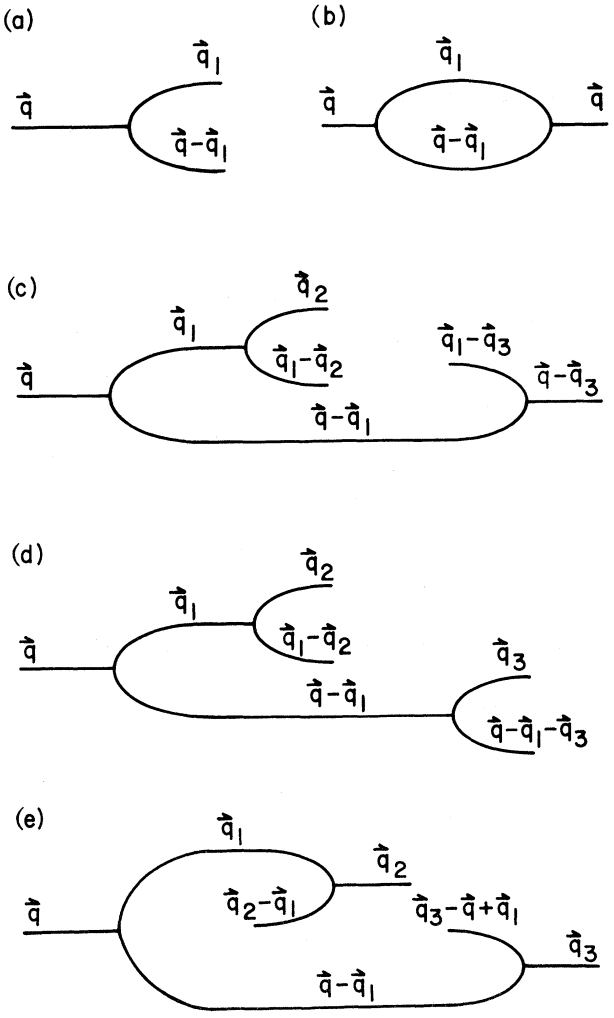

FIG. 3. Basic starting vertex and possible choices for the ends of each leg. Conservation of wave vector has been employed in labeling these diagrams.

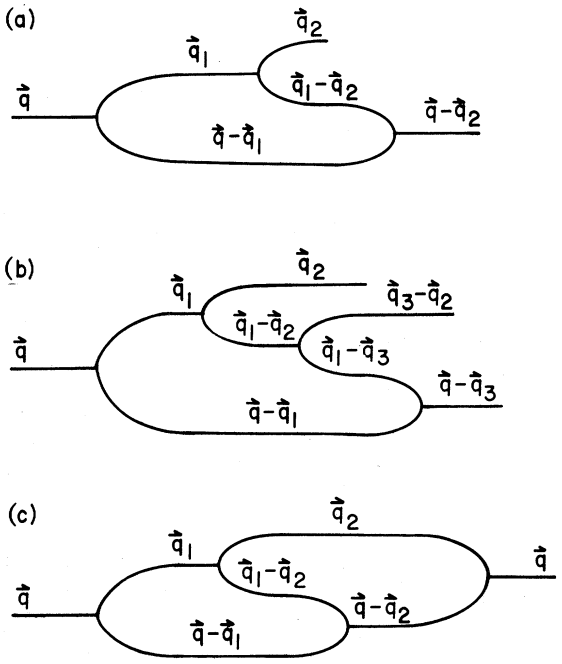

FIG. 4. Continuation of possible diagrams starting from the basic vertex.

$$[V(\vec{q}_1)-V(\vec{q}-\vec{q}_1)][V(\vec{q}_2)-V(\vec{q}_1-\vec{q}_2)][V(\vec{q}_3)-V(\vec{q}-\vec{q}_1-\vec{q}_3)] \quad (10)$$

obtains. With this factor there is no way to obtain an expression of the form of Eq. (7) involving $\vec{q}_1$. The same is true of both legs end in vertices opening to the right as in Fig. 3(e), and in addition, this diagram has too many lines to the left to be completed. Thus we must start with the diagram in Fig. 3(c) which has the factor

$$[V(\vec{q}_1)-V(\vec{q}-\vec{q}_1)][V(\vec{q}_2)-V(\vec{q}_1-\vec{q}_2)][V(\vec{q}_1-\vec{q}_3)-V(\vec{q}-\vec{q}_1)] \quad (11)$$

associated with it. This start is not obviously eliminated because $V(\vec{q}-\vec{q}_1)$ from the last factor can be combined with $V(\vec{q}_2)$ of the second factor and either term of the first factor to yield

$$-[V(\vec{q}_1)V(\vec{q}-\vec{q}_1)-V(\vec{q}-\vec{q}_1)V(\vec{q}-\vec{q}_1)]V(\vec{q}_2). \quad (12)$$

The $\vec{q}_1$ part of this is of the right form and more factors involving $\vec{q}_2$ will occur from the rest of the diagram.

Now note that Fig. 3(c) can be turned into Fig. 4(a) if $\vec{q}_3=\vec{q}_2$. This yields an acceptable form of diagram and, in fact, the arguments of the preceding paragraph can be repeated to continue this diagram where the last factor $V(\vec{q}_2)$ replaces the factor of the starting vertex factor $V(\vec{q}_2)-V(\vec{q}-\vec{q}_2)$. On the other hand, any other construction will lead to factors inconsistent with Eq. (7). For example, the next simplest form, given by Fig. 4(b), has the associated factor

$$-[V(\vec{q}_1)V(\vec{q}-\vec{q}_1)-V(\vec{q}-\vec{q}_1)V(\vec{q}-\vec{q}_1)]\times[V(\vec{q}_2)][V(\vec{q}_1-\vec{q}_3)-V(\vec{q}_3-\vec{q}_2)]f(\vec{q}_2,\vec{q}_3), \quad (13)$$

where $f(\vec{q}_2,\vec{q}_3)$ represents the rest of the diagram and the terms leading up to Eq. (12) have been eliminated. Since the first factor in brackets already satisfies Eq. (7), the rest of the factors cannot include $\vec{q}_1$. Thus we are left with

$$V(\vec{q}_2)V(\vec{q}_3-\vec{q}_2)f(\vec{q}_2,\vec{q}_3). \quad (14)$$

Because of the $V(\vec{q}_3-\vec{q}_2)$, this can never lead to a form consistent with Eq. (7). Of course, Fig. 4(c) is acceptable but would close the diagram. Thus the only acceptable skeleton diagrams are ones which start and end with the basic vertices and whose internal structure consists of segments like those in Figs. 5(a) and 5(b) strung together. The factors to be associated with these diagrams for the isotropic Heisenberg paramagnet to lowest order in $1/Z$ are also given in Fig. 5.

The irreducible but nonskeleton diagrams can be formed by replacing internal lines labeled $\vec{q}_i$ in the skeleton diagrams[2,5] with the moments $M(\vec{q}_i, k)$. Thus the modification of the preceding argument to include all irreducible diagrams is straightforward. The internal lines are merely replaced by other moments exact to lowest order in $1/Z$. However, in the ensuing summations over $\vec{q}_i$, it is still required to lowest order in $1/Z$ that only pairs like those in Eq. (7) appear. Thus only the part of $M(\vec{q}_i, k)$ that is independent of $\vec{q}_i$ need be included in this replacement of internal lines by other moments. For example, with the isotropic Heisenberg paramagnet,

$$M(\vec{q}, 2)=2[V^2(0)-V^2(\vec{q})]. \quad (15)$$

Since the summation of $V^2(\vec{q})$ over the Brillouin zone is zero, the part of $M(\vec{q}_i, k)$ that is independent of $\vec{q}$, can be denoted by $M(k)$, where $M(k)$ is the moment $M(q, k)$ averaged over the Brillouin zone,

$$M(k)=\frac{1}{N}\sum_{\vec{q}}M(\vec{q}, k). \quad (16)$$

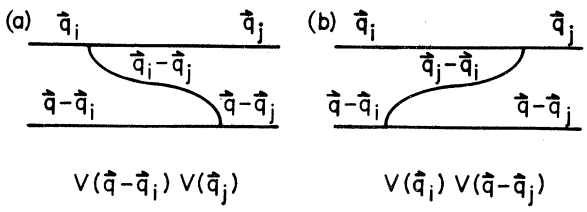

FIG. 5. Allowable internal structure for diagrams contributing to lowest order in $1/Z$ and their associated analytical expressions to order $1/Z$.

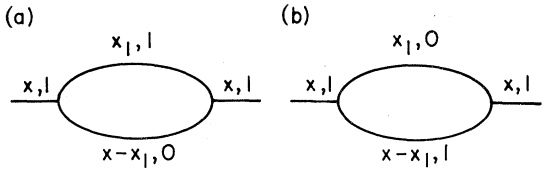

FIG. 6. Lowest-order diagrams for the dipole ($l=1$) correlation function in the isotropic Heisenberg paramagnet. The quantity x_i denotes $(\vec{q}_i, \omega_i)$ and m denotes the azimuthal multipole index.

The translation of these rules for the moments into rules for an integral equation for $\Sigma(\vec{q}, \omega)$ are similar to the ones used in Ref. 2. The rules for $\Sigma_{\alpha\beta}(\vec{q}, t)$ are as follows: (i) Draw all distinct skeleton diagrams which start with a basic vertex with a $\vec{q}$, α-type line, end with a basic vertex with a $\vec{q}$, β-type line, and whose internal structure is made up of segments like those in Figs. 5(a) and 5(b) strung together. (ii) Label the internal vertices t_i, α_i and the internal momenta $\vec{q}_i$. (iii) Associate the appropriate numerical factor with each vertex and replace the internal lines between vertices α_i, t_i and α_j, t_j with $G_{\alpha_i\alpha_j}(t_i - t_j)$, where $G(t)$ is the local or $\vec{q}$-independent solution defined by moments as in Eq. (16). (iv) Multiply each diagram by $(-i)^{n_v+1}$ where n_v is the number of internal vertices, integrate over internal times, and sum over internal wave vectors.

The rules for $\Sigma_{\alpha\beta}(t)$, the self-energy associated with the $\vec{q}$-independent correlation function $G_{\alpha\beta}(t)$, are similar except we take only the $\vec{q}$-independent part. In practice, this reduces to modifying step (i) of the preceding paragraph to use only diagrams whose internal segments like those in Figs. 5(a) and 5(b) alternate. That is, only extended segments like those in Fig. 8(a) contribute in such a way so as to be independent of $\vec{q}$.

The above procedure does not in itself give a finite equation for G in that there are still an infinite number of diagrams for Σ. However, it is not hard to believe that the subset of diagrams now needed to obtain exact results to lowest order in $1/Z$ can be summed. In Sec. III we will show how they can be summed for the isotropic Heisenberg paramagnet. Extensions to other systems are straightforward but tedious.

III. DISCUSSION

In this section we shall explicitly sum all of the diagrams to lowest order in $1/Z$ for the isotropic Heisenberg paramagnet and discuss some applications to other spin systems. For the isotropic Heisenberg paramagnet, all of the correlation functions $G_{\alpha\beta}$ are diagonal ($\alpha=\beta$) and, if we consider only the dipole-dipole ($l=1$) correlation functions, all three ($m=1, 0, -1$) of them are identical.

First consider the equations for the local or q-independent correlation function $G_l(\omega)$ whose self-energy is $\Sigma_l(\omega)$. The diagrams for Σ_l can be expressed as simply in ω space as in t space and the frequencies flow just as the wave vectors do. In what follows we shall use the shorthand notation x_i where $x_i \equiv (\vec{q}_i, \omega_i)$. The lowest-order diagram, given by Fig. 6(a), yields

$$-2iV^2(0)\int\frac{d\omega_1}{2\pi}\,G_l(\omega_1)\,G_l(\omega-\omega_1)\,. \tag{17}$$

The factor of two comes from the $\vec{q}$-independent part of

$$\frac{1}{N}\sum_{\vec{q}_1}[V(\vec{q}_1)-V(\vec{q}-\vec{q}_1)]^2 = 2[V^2(0)-V^2(\vec{q})]\,. \tag{18}$$

Figure 6(b) is not a distinct diagram because it can be obtained from Fig. 6(a) by a simple rotation. The higher-order diagrams start like those in Figs. 7. There is a factor of two because diagrams Figs. 7(a) and 7(b) are distinct. By the rules discussed in Sec. II, the middle portion of the higher-order diagrams look like Fig. 8(a), and the contribution to $\Sigma_l(\omega)$ from all terms with $2n$ vertices is

$$\left(-2iV^2(0)\int\frac{d\omega_1}{2\pi}\,G_l(\omega_1)\,G_l(\omega-\omega_1)\right)$$
$$\times\prod_{k=2}^{n+1}\left(-V^2(0)\int\frac{d\omega_k}{2\pi}\,G_l(\omega_k)\,G_l(\omega-\omega_k)\right.$$
$$\left.\times G_l(\omega_k+\omega_{k-1}-\omega)\right). \tag{19}$$

These terms can be formally summed to yield

$$\Sigma_l(\omega) = -2iV^2(0)\int\frac{d\omega_1}{2\pi}\,G_l(\omega_1)\,G_l(\omega-\omega_1)\,F_l(\omega,\omega_1)\,, \tag{20a}$$

$$F_l(\omega,\omega_1) = 1 - V^2(0)\int\frac{d\omega_1}{2\pi}\,G_l(\omega_1+\omega_2-\omega)$$
$$\times G_l(\omega_2)\,G_l(\omega-\omega_2)\,F_l(\omega,\omega_2)\,, \tag{20b}$$

$$G_l(\omega) = i/[\omega-\Sigma_l(\omega)]\,. \tag{20c}$$

These equations can be solved self-consistently to

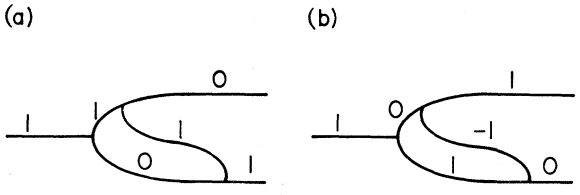

FIG. 7. Start of the higher-order diagrams for the Heisenberg paramagnet with only the azimuthal multipole index m indicated.

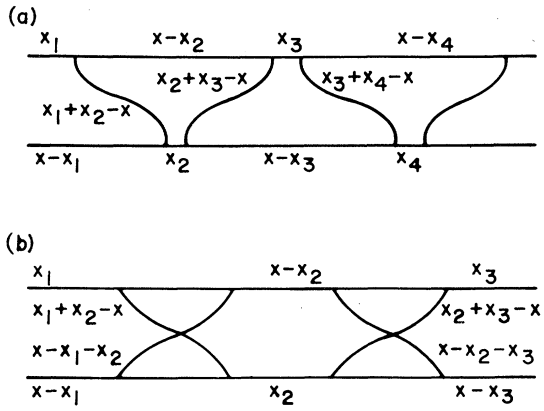

FIG. 8. Internal structure of diagrams contributing to (a) $\Sigma_l(\omega)$ and (b) $\Sigma(\vec{q}, \omega)$. The quantity x_i denotes $(\vec{q}_i, \omega_i)$.

obtain the local solution $G_l(\omega)$. The quantity $F_l \times(\omega, \omega_1)$ is essentially a form factor and if F is set equal to one, Eqs. (20) describe the local correlation function in the bubble approximation.

The equations for $\Sigma(\vec{q}, \omega)$ are somewhat more complex because the internal segments of the diagrams can consist of Figs. 5(a) and 5(b) in any sequence. The first term for $\Sigma(\vec{q}, \omega)$ is

$$(-2i)[V^2(0) - V^2(\vec{q})] \int \frac{d\omega_1}{2\pi} G_l(\omega_1) G_l(\omega - \omega_1) . \tag{21}$$

A general internal segment can be represented schematically by Fig. 8(b). The meaning of the crossed lines is that either one of each pair of crossed line enters a given diagram contributing either $G_l(\omega_i + \omega_{i+1} - \omega)$ or $G_l(\omega - \omega_i - \omega_{i+1})$. A simple analysis shows that the factor $V^2(0)$ occurs when two successive cross lines run different ways [one like the Fig. 5(a) and one like in Fig. 5(b)] and the factor $V^2(\vec{q})$ when two successive cross lines run the same way [both like in Fig. 5(a) or both like in Fig. 5(b)]. A more tedious but straightforward analysis yields the following set of equations for $G(g, \omega)$:

$$\Sigma(\vec{q}, \omega) = (-2i)[V^2(0) - V^2(\vec{q})] \int \frac{d\omega_1}{2\pi} G_l(\omega_1) G_l(\omega - \omega_1) + 2i[V^2(0) - V^2(\vec{q})]^2 \int \frac{d\omega_1}{2\pi} \frac{d\omega_2}{2\pi} G_l(\omega_1) G_l(\omega - \omega_1)$$
$$\times G_l(\omega_1 - \omega_2 - \omega) G_l(\omega_2) G_l(\omega - \omega_2) F_{11}(\omega, \omega_2; \vec{q}) , \tag{22a}$$

$$F_{ij}(\omega, \omega_2; \vec{q}) = F^0_{ij} - \int \frac{d\omega_3}{2\pi} G_l(\omega_3) G_l(\omega - \omega_3) M_{ik}(\omega_2, \omega_3, \omega; \vec{q}) F_{kj}(\omega, \omega_3; \vec{q}) , \tag{22b}$$

where the repeated Latin subscripts imply matrix multiplication and

$$F^0_{ij} = \begin{bmatrix} 1 & 1 \\ 1 & 1 \end{bmatrix} , \tag{22c}$$

$$M_{ij}(\omega_2, \omega_3, \omega; \vec{q}) = \begin{bmatrix} V^2(0) G(\omega_2 + \omega_3 - \omega) & V^2(\vec{q}) G(\omega - \omega_2 - \omega_3) \\ V^2(\vec{q}) G_l(\omega_2 + \omega_3 - \omega) & V^2(0) G_l(\omega - \omega_2 - \omega_3) \end{bmatrix} . \tag{22d}$$

Equations (20) and (22) describe a solution for $G(\vec{q}, \omega)$ all of whose moments are exact to order $1/Z$.

As one can see, the equations for the dipole spin correlation function for the high-temperature isotropic Heisenberg paramagnet are quite involved. The equations for any other spin system will be even worse. For example, we are presently applying the formalism to obtain equations for the dipolar paramagnet. However, we estimate that the solution to these equations will take more computer time to solve than the corresponding equations for the isotropic Heisenberg paramagnet by more than an order of magnitude. Thus we chose to apply the formalism first to the Heisenberg paramagnet because the equations are the simplest in this case and the feasibility of the method could be studied with a limited computer budget.

We have computed the local spectral function $g_b(\omega)$ using the bubble approximation and the local spectral function $g_f(\omega)$ using the full approximation given by Eqs. (20). The results of these computations are shown in Fig. 9. The zeroth and second moments of these functions are identical but the higher moments of $g_f(\omega)$ are larger than the corresponding moments of $g_b(\omega)$. It is interesting to note that $g_f(\omega)$ is greater than $g_b(\omega)$ at zero frequency and also at asymptotically larger frequencies. Thus, in this case, the function with larger higher moments is also larger at $\omega = 0$.

The local spectral function $g_b(\omega)$ is not precisely the autocorrelation function calculated by Blume and Hubbard.[1] This is because we have neglected terms of order $1/Z$ in solving the q-dependent bubble approximation. In fact, $g_b(\omega)$ is the Fourier transform of the solution of the equation derived by Resibois and De Leneer.[4] However, in our scheme the local spectral function is an intermediate step

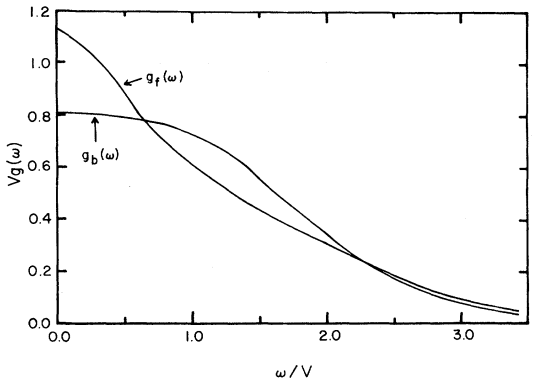

FIG. 9. Comparison of the local or $\vec{q}$-independent spectral functions computed in the bubble approximation, $g_b(\omega)$, and in the full approximation given by Eqs. (20), $g_f(\omega)$, for the isotropic Heisenberg paramagnet. Frequencies are in units of $V=[V^2(0)]^{1/2}$.

in our calculation and not a final result to be compared with experiment. The bubble approximation to order $1/Z$ is recovered by using Eq. (20a) with $F_1(\omega, \omega_1)=1$ and then the first line of Eq. (22a). The spectral function $g_b(\vec{q}, \omega)$ obtained in this way is within a few percent of the spectral function obtained by Blume and Hubbard. The same holds true for the autocorrelation function obtained by averaging $g_b(\vec{q}, \omega)$ over $\vec{q}$.

Our comparison with experimental results is limited to a calculation of the spin diffusion coefficient. This quantity can be computed from $G_1(\omega)$ without calculating $F_{ij}(\omega, \omega_2; \vec{q})$, since only the first term of Eq. (22a) is significant for small $\vec{q}$. The spin diffusion coefficient obtained from the full approximation is only 4% lower than the experimentally measured[10] value for $RbMnF_3$ compared to the value obtained from the bubble approximation which is 11.5% too low.

*Research supported in part by the National Science Foundation.

[1]M. Blume, and J. Hubbard, Phys. Rev. B 1, 3815 (1970).
[2]Charles W. Myles and Peter A. Fedders, Phys. Rev. B 9, 4872 (1974).
[3]F. Wegner, Z. Phys. 216, 433 (1968); 218, 260 (1969).
[4]P. Resibois and M. De Leneer, Phys. Rev. 152, 305 (1966); 152, 318 (1966); 178, 806 (1969); 178, 819 (1969).
[5]G. F. Reiter, Phys. Rev. B 5, 222 (1972).
[6]See also, H. S. Bennett and P. C. Martin, Phys. Rev. 138 A608 (1965); F. B. Mclean and M. Blume, Phys. Rev. B 7, 1149 (1973); G. F. Reiter, *ibid* 2, 3325 (1973); D. L. Huber, *ibid.* 6, 3180 (1972) and references therein.
[7]Peter A. Fedders, Charles W. Myles, and C. Ebner, in Proceedings of the 20th Annual Magnetic Materials and Magnetism Conference, 1974 (unpublished).
[8]M. Blume (private communication).
[9]Peter A. Fedders (unpublished).
[10]C. G. Windsor, G. A. Briggs, and M. Kestigan, J. Phys. C 1, 940 (1968).